Applied Catalysis B: Environmental 152–153 (2014) 82–87

Contents lists available at ScienceDirect

Applied Catalysis B: Environmental

journal homepage: www.elsevier.com/locate/apcatb

Photocatalytic oxidation of gaseous ammonia over fluorinated TiO_2 with exposed (0 0 1) facets

Hongmin Wu, Jinzhu Ma, Yaobin Li, Changbin Zhang*, Hong He

Research Center for Eco-Environmental Sciences, Chinese Academy of Sciences, Beijing 100085, China

ARTICLE INFO

Article history:
Received 17 September 2013
Received in revised form 6 January 2014
Accepted 13 January 2014
Available online 23 January 2014

Keywords:
Photocatalysis
NH_3
Fluorination
TiO_2
Indoor air quality

ABSTRACT

A surface-fluorinated TiO_2 (F–TiO_2) catalyst was synthesized by a hydrothermal method using hydrofluoric acid (HF) solution as a capping agent, and defluorinated TiO_2 (D-TiO_2) was next obtained by washing the F–TiO_2 with NaOH solution. The as-prepared catalysts were tested for the photocatalytic oxidation (PCO) of gaseous NH_3 under UV light. The F–TiO_2 catalyst exhibited remarkable activity for NH_3 removal, about twice as high as that of the commercial catalyst P25. In contrast, D-TiO_2 showed an obvious decrease in PCO activity. The catalysts were characterized by X-ray diffractometry (XRD), Brunauer–Emmett–Teller (BET) adsorption analysis, High-resolution Transmission electron microscopy (HR-TEM), and X-ray photoelectron spectroscopy (XPS). The results showed that the surface fluorination process formed the surface ≡Ti–F group and also increased the percentage of reactive (0 0 1) facets to about 50%; the surface defluorination removed the fluorine (F) element from the F–TiO_2 surface but showed no influence on the percentage of reactive (0 0 1) facets. By comparing the specific activities of the catalysts, we found that both the active (0 0 1) facets and the surface ≡Ti–F group contributed to the improvement of the PCO activity, while the surface ≡Ti–F group plays the dominant role. The ≡Ti–F group could retard the recombination of photogenerated electrons and holes, which is possibly the major reason for the excellent activity of the F–TiO_2 catalyst.

1. Introduction

More and more attention has been paid to indoor air quality, since people spend almost 90% of their time inside buildings [1]. Gaseous ammonia (NH_3), released from walls containing urea or ammonia compound-based antifreeze admixtures, is one of the major indoor air pollutants, particularly in China [2,3]. NH_3 is an alkaline gas with a pungent odor and is harmful to the environment and people's health. Long-time exposure to NH_3 can cause irritation of the skin, throat, lungs and eyes, affect the respiratory system and even cause permanent damage to the organs [3]. Therefore, it is of great interest to eliminate indoor air NH_3 to meet environmental regulations and health needs.

NH_3 can be eliminated by traditional remediation techniques, such as adsorption and ventilation, but they cannot eliminate NH_3 completely [4]. Selective catalytic oxidation (SCO) is an effective method to degrade NH_3, but the oxidation reaction generally requires a high temperature [5–7]. Photocatalytic oxidation (PCO) could eliminate the indoor air pollutants such as formaldehyde and volatile organic compounds under ultraviolet (UV) light irradiation at ambient temperature; therefore, it is a promising method for indoor air NH_3 destruction [8–11]. A few studies have been focused on the photocatalytic removal of gaseous NH_3. Several types of modified TiO_2-based photocatalysts such as TiO_2-activated carbon composites [12,13], woven fabric-supported P25 [14,15] and latex paint-supported film nano-TiO_2 [16,17] have been evaluated for the PCO of NH_3 under UV light irradiation. The product distribution during the PCO of NH_3 has been investigated by FTIR or GC/GC–MS, and N_2 was found to be the main gaseous product; N_2O, NO_2^- and NO_3^- were registered as the major by-products [12,18–20]. In general, the catalysts studied for the PCO of NH_3 reactions were anatase TiO_2 supported catalysts or the commercial catalyst P25. There are few studies focusing on the development of new types of catalysts for improving the photocatalytic activity of NH_3 removal.

Recently, anatase TiO_2 with exposed (0 0 1) facets has drawn great attention since Yang et al. prepared anatase TiO_2 microcrystals with 47% highly reactive (0 0 1) facets [21–30]. The average surface free energy of (0 0 1) facets is 0.90 J/m^2, which is higher than those of (1 0 0) (0.53 J/m^2) and (1 0 1) facets (0.44 J/m^2) [31]. The majority of exposed facets of anatase TiO_2 are normally (1 0 1) due to it having the lowest surface energy under common conditions. In controllable synthesis of TiO_2 with exposed (0 0 1) facets, fluorine has been commonly used as a morphology-controlling agent to lower the surface energy in order to expose the reactive

* Corresponding author. Tel.: +86 10 62849121; fax: +86 10 62849121.
E-mail address: cbzhang@rcees.ac.cn (C. Zhang).

0926-3373/$ – see front matter © 2014 Elsevier B.V. All rights reserved.
http://dx.doi.org/10.1016/j.apcatb.2014.01.021

(0 0 1) facets [23,32,33]. Anatase TiO_2 with a high percentage of the reactive (0 0 1) facets has exhibited excellent photoreactivity, even much better than pure anatase TiO_2 or commercial P25 in photocatalytic reactions, such the oxidation of acetone [23], OH radical generation [24] and the degradation of methylene orange (MO) [34] and methylene blue (MB) [35], etc. However, it is also reported that, compared with the other two facets, (0 0 1) facets are not always more reactive for some reactions, such as the reaction of hydrogen generation under UV light irradiation [36,37]. In addition, surface fluorination also showed some influence on the activity by retarding the recombination of the photogenerated electrons and holes, since the negative electrons and positive holes can selectively migrate to the specific exposed crystal face [23].

In this study, anatase TiO_2 with exposed (0 0 1) facets was synthesized via a hydrothermal route using HF as capping agent [23]. The catalysts were tested for the PCO of NH_3 reaction under UV light irradiation at room temperature. The effects of both the (0 0 1) facet percentage and the surface fluorination on the TiO_2 activity for the PCO of NH_3 reaction were examined in detail.

2. Experimental

2.1. Catalyst preparation

Pure anatase TiO_2 and fluorinated TiO_2 (F–TiO_2) were prepared using a hydrothermal route similar to that reported by Yu et al. [23]. 3 mL of distilled water or hydrofluoric acid solution (with a concentration 40 wt%) (AR, China) were dropwise added into 25 mL of tetrabutyl titanate ($Ti(OC_4H_9)_4$, CP, China) in a Teflon-lined autoclave at room temperature and under magnetic stirring. Then the Teflon-lined autoclave was kept at 190 °C for 24 h. After hydrothermal reaction, the precipitates were collected, washed with ethanol and distilled water four times, and then dried in an oven at 60 °C overnight.

The defluorinated TiO_2 (D-TiO_2) was next obtained by washing the F–TiO_2 with NaOH solution. 1000 mg of the powder F–TiO_2 was reacted in 50 mL of 0.1 M NaOH solution under magnetic stirring for 10 h in the dark. Then the mixture was washed by dilute HCl solution and distilled water several times until no F^- was detected in the filtrate. The collected precipitant was dried at 60 °C overnight.

2.2. Characterization of catalysts

Nitrogen adsorption–desorption isotherms were obtained at −196 °C using a Quantasorb-18 automatic instrument (Quanta Chrome Instrument Co). Specific surface areas were computed from these isotherms by applying the Brunauer–Emmett–Teller (BET) method. The pore size distribution was calculated from the desorption branch of the nitrogen isotherm by the BJH (Barrett–Joyner–Halenda) method. Powder X-ray diffraction (XRD) measurements of the catalysts were carried out on a PANalytical X'Pert Pro diffractometer using Cu $K\alpha$ radiation operating at 40 kV and 40 mA. The patterns were taken over the 2θ range from 10° to 90° with a step size of 0.026°. Transmission electron microscopy (TEM) and high-resolution transmission electron microscopy (HRTEM) images were obtained on a JEM-2011 electron microscope (JEOL, Japan). Field emission scanning electronic microscopy (FE-SEM) measurements were performed on a SU-8020 electron microscope (Hitachi, Japan). Diffuse-reflectance UV–vis spectra were obtained on a UV-1700 (SHIMADZU) spectrometer. The range was 190–800 nm and the scan rate was 120 nm/min. Photoluminescence (PL) spectra were measured on a Fluorescence Spectrophotometer (F-4500, Hitachi, Japan). The exciting wavelength was 300 nm, the scanning speed was 240 nm/min, the PMT voltage was 400 V and the widths of the excitation and emission slits were 5.0 nm. X-ray photoelectron spectroscopy (XPS) of the catalysts was performed on a scanning X-ray microprobe (Axis Ultra, Kratos Analytical Ltd.) using Al $K\alpha$ radiation (1486.7 eV). All the binding energies were calibrated using the C 1s peak (BE = 284.8 eV) as standard.

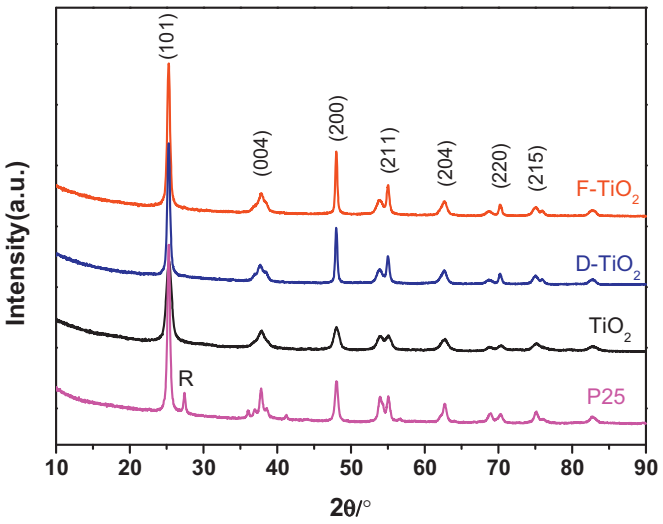

Fig. 1. XRD patterns of pure TiO_2, F–TiO_2, D-TiO_2 and P25 catalysts.

2.3. Catalytic evaluation of catalysts

The catalyst evaluations for photocatalytic removal of gaseous NH_3 were performed in a black-colored box with a 500 W ultraviolet high pressure mercury lamp in a continuous flow system. The intensity of the UV light irradiation with peak wavelength at 365 nm on the catalysts' surface was 0.46 mW/cm^2. There was a fan above the lamp and a circulated cooling system under the vessel to control the reaction temperature at 24 °C. 100 mg catalyst was dispersed in water and then the turbid solution was spread over a round stainless steel sample dish with diameter of 5.5 cm. The sample must be dry before being used. The reactant gas was 50 ppm NH_3, 20 vol% O_2, and balance N_2 with a total flow rate of 200 mL/min, and the relative humidity was 50%. The inlet and outlet gases were monitored by an FTIR (Nicolet 380) equipped with a 2 m gas cell.

3. Results and discussion

3.1. Phase structure and morphology

XRD patterns of TiO_2 catalysts were measured to characterize the bulk crystalline structures of the TiO_2 samples, and the results are shown in Fig. 1. Different from the commercial P25, the as-prepared catalysts only presented the anatase phase with peaks at 2θ = 25.3° (1 0 1), 37.8° (0 0 4), 48.1° (2 0 0), 54.0° (1 0 5) and 55.1° (2 1 1) (JCPDS no. 21-1272), with good crystallinity. The crystal sizes of TiO_2 were calculated from the half-width of peaks using Scherrer's formula ($d = 0.9\lambda/\beta\cos\theta$) and the results are shown in Table 1. It can be seen that the crystal size of F–TiO_2 is larger than that of pure TiO_2 as a result of the fluoride addition, which can facilitate the growth of crystallites [38]. The defluorination process had no influence on the crystal structures of samples; D-TiO_2 showed an XRD pattern and crystal size similar to that of F–TiO_2.

FE-SEM and HR-TEM images of the catalysts are shown in Fig. 2. From the FE-SEM image of the pure TiO_2 (Fig. 2a), we can see that the TiO_2 particle is regular in shape with average particle size of about 11 nm, which is in accordance with the results of XRD. The

Table 1
Structural parameters of pure TiO_2, F–TiO_2, D-TiO_2 and P25.

Sample	SSA (m^2/g)	Pore diameter (nm)	Pore volume (cm^3/g)	Crystal size (nm)	Percentage of (0 0 1) (%)
TiO_2	140.1	5.44	0.19	11.5	20.1
F–TiO_2	86.2	14.8	0.32	19.4	49.3
D-TiO_2	86.7	17.7	0.38	19.5	49.3
P25	59.1	11.8	0.17	20.8	17.7

HR-TEM image of pure TiO_2 (Fig. 2b) shows that the lattice spacing is 0.35 nm, corresponding to the (1 0 1) planes of anatase TiO_2, indicating that the pure TiO_2 has mainly (1 0 1) facets exposed. The FE-SEM and HR-TEM images of F–TiO_2 (Fig. 2c and d) show that the as-prepared F–TiO_2 consists of regular sheet-shaped structures, with an average side length of about 30 nm and an average thickness of about 10 nm. In addition, the HR-TEM image (Fig. 2d) directly shows that the lattice spacing parallel to the top and bottom facets is 0.235 nm, corresponding to the (0 0 1) planes, indicating that the exposed facets for F–TiO_2 are predominantly (0 0 1). The

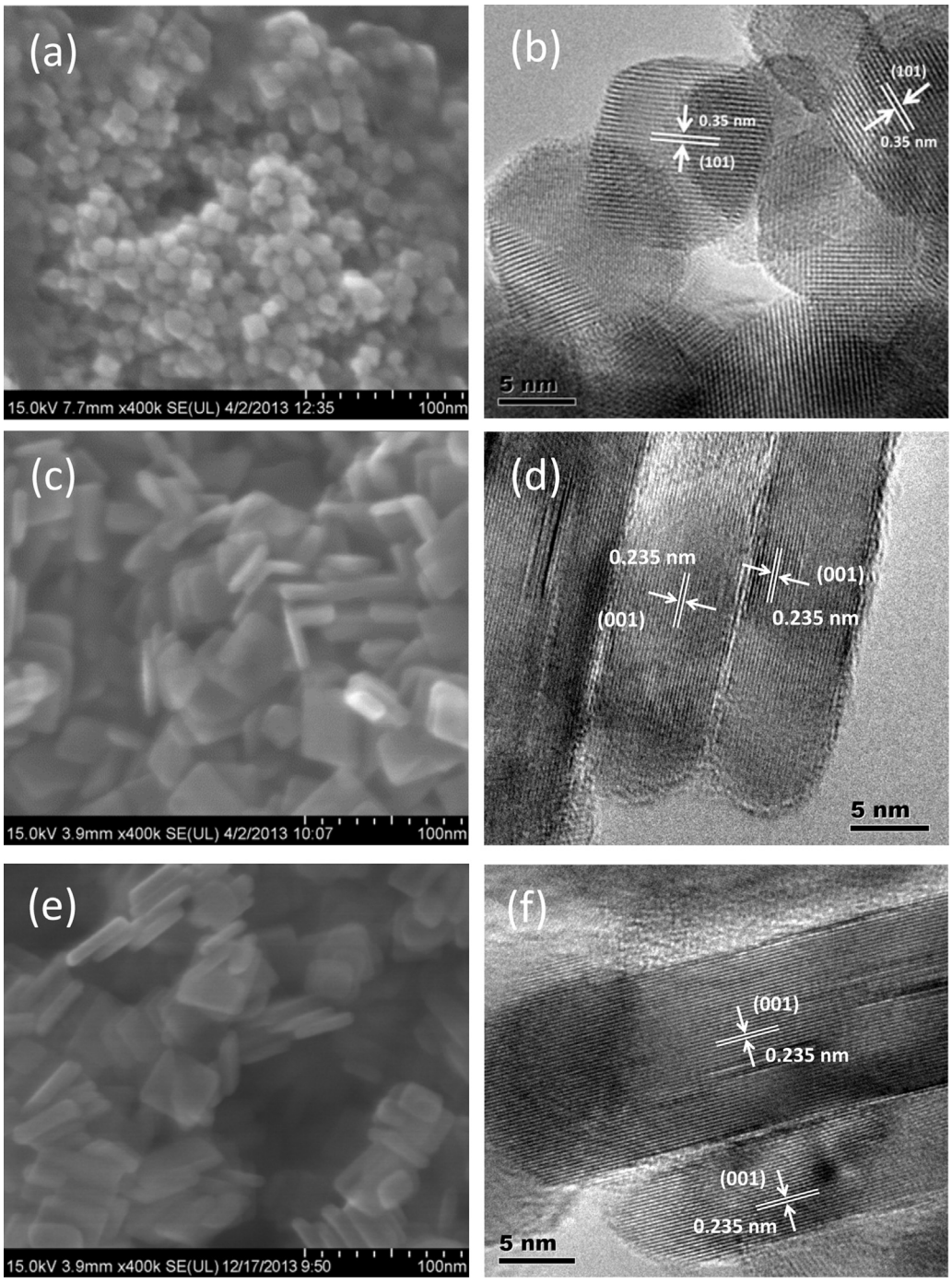

Fig. 2. FE-SEM image and HR-TEM image of pure TiO_2 (a and b), F–TiO_2 (c and d) and D-TiO_2 (e and f) catalysts.

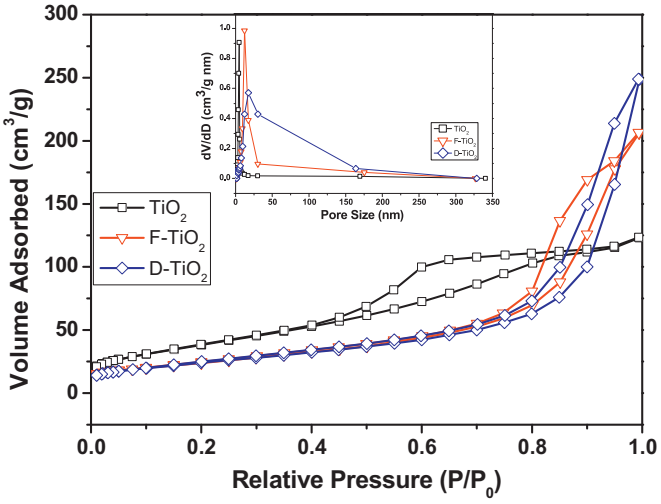

Fig. 3. Nitrogen adsorption–desorption isotherms of the TiO_2 samples and their pore size distribution curves (inset).

further defluorination process did not change the crystal structure and morphology of D-TiO_2, and its active (0 0 1) facets remained intact (Fig. 2e and f). Based on the XRD results, SEM and HR-TEM images, we calculated the percentage of exposed (0 0 1) facets [35,37], and the data are shown in Table 1. It is indicated that the percentage of (0 0 1) facets for F–TiO_2 is 49.3%, which is much higher than that of pure TiO_2 (20.1%). Moreover, the D-TiO_2 catalyst had a percentage of (0 0 1) facets equal to the F–TiO_2 catalyst, further proving that the defluorination process had no effect on the crystal structure of the samples.

3.2. BET surface area and pore size distribution

Nitrogen adsorption–desorption isotherms were measured to determine the textural structures of TiO_2 samples and the results are shown in Table 1 and Fig. 3. The as-prepared anatase TiO_2 presented a 140.1 m^2/g BET surface area, 5.44 nm pore diameter and 0.19 cm^3/g pore volume. The surface fluorination resulted in a sharp drop in the BET surface area but a sharp increase in the pore size and pore volume of F–TiO_2 due to growth of TiO_2 crystallites [23,39]. In contrast, the defluorination process did not induce much difference in BET surface area, pore diameter and pore volume of samples. As shown in Fig. 3, the isotherm of pure TiO_2 was type IV and the hysteresis loop was of type H2, indicating that the pure TiO_2 might mainly consists of the ink-bottle pores. The pore size distribution of the pure TiO_2 presented a narrow range of 2.0–7.0 nm with a peak of about 5 nm. The fluorination resulted in the change of the hysteresis loop from type H2 to H3, showing that the pore structure is dramatically altered after the fluorination and the slit-like pores is formed due to the aggregation of TiO_2 nanosheets. In addition, the pore size distribution of F–TiO_2 is wider than that of pure TiO_2, indicating the coexistence of both mesopores and macropores, which can facilitate the transport of reactant and product molecules in photocatalytic reactions [23]. The D-TiO_2 also showed the H3 type hysteresis loop but with a wider pore size distribution than that of F–TiO_2 possibly due to the fluorine removal in the pores.

3.3. XPS analysis

XPS spectra of pure TiO_2, F–TiO_2 and D-TiO_2 are shown in Fig. 4. These catalysts all contained C, Ti, and O elements, with sharp photoelectron peaks appearing at binding energy 285 eV (C 1s), 458 eV (Ti 2p) and 531 eV (O 1s). The C element is ascribed to residual carbon. The fluoride peak at binding energy 684.5 eV (F 1s) only appears in the F–TiO_2 sample, indicating the formation of surface fluoride (≡Ti–F) by a ligand exchange reaction between F^- and the surface hydroxyl group on the TiO_2 surface [40–44]. No peak for F^- ions in the lattice at 688.5 eV was observed in the spectra, because the hydrothermal process could prevent the substitution of F^- for O^{2-} in the lattice of TiO_2 [21,39,40,45]. The fluoride peak in the D-TiO_2 almost disappeared after defluorination, indicating that the surface fluorine atoms were removed by NaOH washing for 10 h [46].

3.4. UV–vis and PL analysis

UV–vis diffuse reflectance spectra were measured to investigate the optical properties of the catalysts, and the results are shown in Fig. 5. The pure TiO_2, F–TiO_2 and D-TiO_2 showed similar adsorption edge regions with an obvious blue shift compared with P25, indicat-

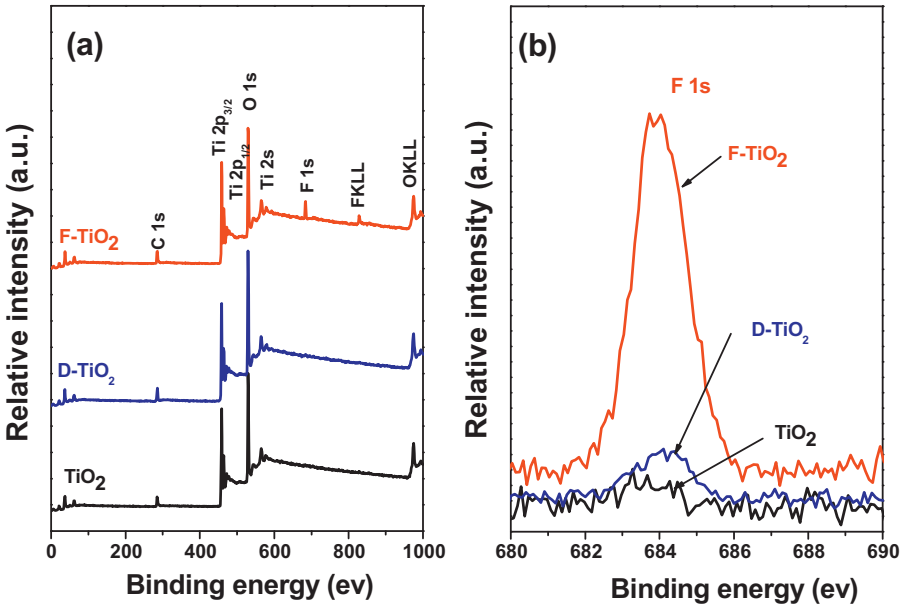

Fig. 4. XPS survey spectra (a) and high resolution XPS spectra of F 1s (b) of pure TiO_2, F–TiO_2 and D-TiO_2.

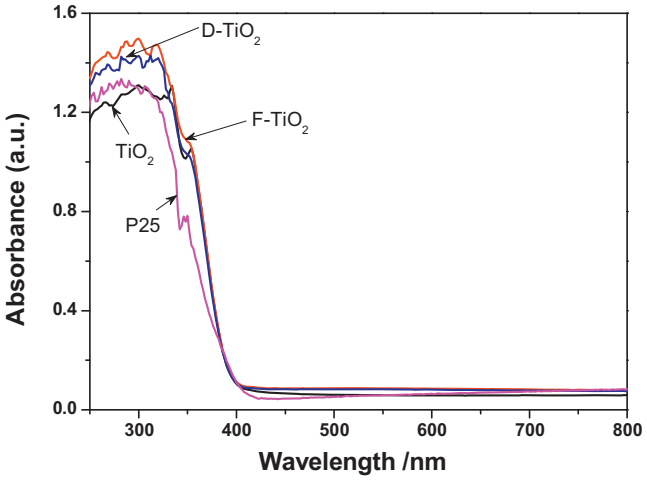

Fig. 5. UV–vis diffuse reflection spectra of pure TiO_2, F–TiO_2, D-TiO_2 and P25.

ing that as-prepared catalysts have a wider band gap than P25. It has been reported that a wider band gap may cause a higher oxidation power for the photo-induced holes [27]. Moreover, the absorbance intensity of the F–TiO_2 catalyst in the UV region is strongest among the series of samples, which will favor improvement of the photocatalytic activity.

Photoluminescence (PL) spectra of catalysts were next measured to investigate the efficiency of charge carrier trapping, migration, and transfer and the separation of photogenerated electron–hole pairs [47]. It was reported that a weaker PL emission signal is commonly indicative of higher photocatalytic activity [48,49]. Fig. 6 shows the measured PL spectra, and all samples presented similar emission bands. The broad emission band at around 400 nm is attributed to the emission of the band gap transition, and the other five peaks ranging from 440 nm to 500 nm are due to surface oxygen vacancies, impurities and defects, respectively [50]. It is noteworthy that the F–TiO_2 sample has the lowest PL signals among the as-prepared catalysts and P25. It has been reported that the ≡Ti–F group on the F–TiO_2 surface could act as an electron-trapping site to trap the photo-generated electrons, by holding trapped electrons and then transferring them to O_2 adsorbed on the TiO_2 surface [23,34,39]. Thus, the ≡Ti–F group accounts for the very low PL spectra intensity of F–TiO_2. In addition, the D-TiO_2 catalyst still showed a lower PL signal than pure TiO_2 and P25, which should be attributed to the presence of about 50% percentage of

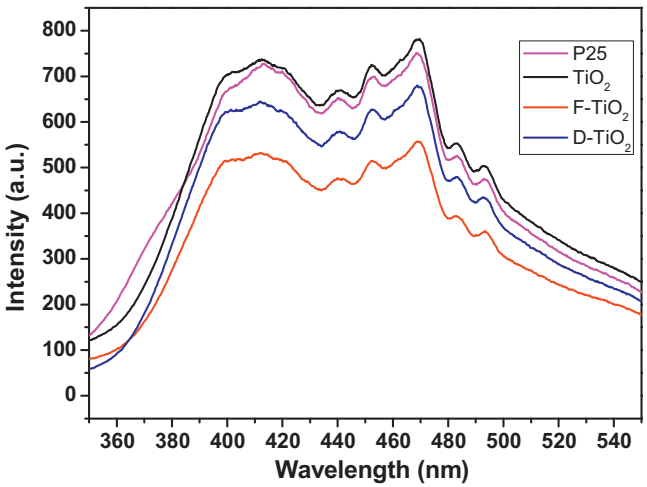

Fig. 6. PL spectra of pure TiO_2, F–TiO_2, D-TiO_2 and P25.

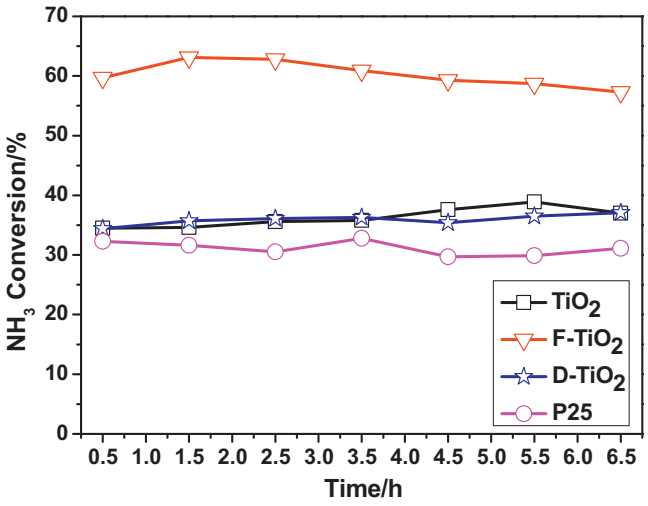

Fig. 7. Activities of TiO_2, F–TiO_2, D-TiO_2 and P25 catalysts for the PCO of NH_3 as a function of UV light irradiation time.

exposed (0 0 1) facets, because a percentage of (0 0 1) facets is also beneficial for the transfer and separation of photo-generated electrons and holes [23].

3.5. Photocatalytic activity test

The prepared catalysts were evaluated for the PCO of NH_3 under UV light (365 nm) at room temperature. Fig. 7 presents the NH_3 conversion with time on-stream over all catalysts and Fig. 8 shows the average NH_3 conversion of the catalysts. All the catalysts showed stable activities during the tests. It is well known that P25 has excellent photocatalytic activity. Compared with P25, the as-prepared catalysts using the hydrothermal method presented better activity for the PCO of NH_3. The removal efficiency of the pure TiO_2 catalyst was about 35%. The F–TiO_2 catalyst presented the best photocatalytic activity with above 60% NH_3 removal efficiency, which is about twice as high as that of P25. The defluorination process resulted in a obvious decrease in photocatalytic activity, and the NH_3 removal efficiency over the D-TiO_2 catalyst was only about 36%, similar to that of the pure TiO_2 catalyst.

As shown in Table 1, the BET surface areas of as-prepared catalysts were very different from each other. Therefore, we calculated

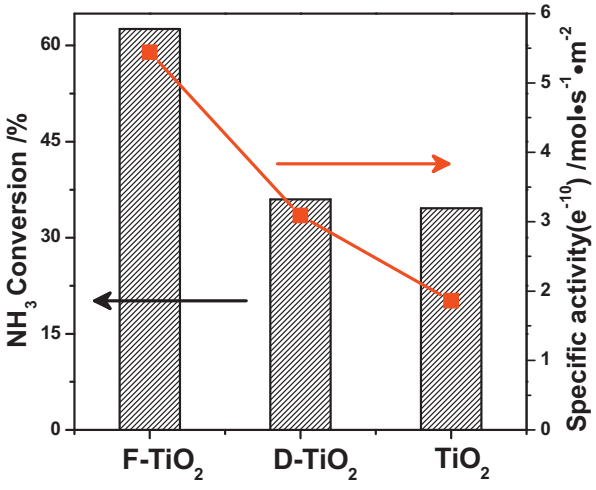

Fig. 8. Comparison of the average photocatalytic activities (column) and the specific activities (line + symbol) of TiO_2, F–TiO_2 and D-TiO_2 catalysts.

the specific activities normalized by surface area to exclude the effect of BET surface area on activity, and the results are given in Fig. 8. The F–TiO_2 exhibited the highest specific activity among the samples. The specific activity sharply dropped after defluorination, however, the D-TiO_2 still presented much higher specific activity than the pure TiO_2. These findings show that the PCO of NH_3 reaction is closely related to both the percentage of exposed active (0 0 1) facets and the surface fluorination.

It has been reported that the (0 0 1) surface of anatase TiO_2 is more reactive than the stable (1 0 1) surface, and is normally the dominant active site for the PCO reactions [23,51]. In addition, the surface ≡Ti–F group can reduce the recombination rate of the photo-generated electrons and holes, thus leading to the better photocatalytic activity. Therefore, the surface fluorinated F–TiO_2 catalyst, with a high percentage of exposed active (0 0 1) facets, exhibited excellent activity for the PCO of NH_3. The defluorination process removed the ≡Ti–F groups from the catalyst surface and partially lost the ability to decrease the recombination rate of electrons and holes; however, the 50% percentage of active (0 0 1) facets remained unchanged during the process. Therefore, although the specific activity of the D-TiO_2 obviously dropped after defluorination, it was still much higher than the pure TiO_2. In addition, as shown in Fig. 8, the specific activities of F–TiO_2, D-TiO_2 and pure TiO_2 were about 5.44×10^{-10}, 3.06×10^{-10} and 1.86×10^{-10} mol/s/m^2, respectively. It is clear that the surface ≡Ti–F group plays a more important role than the active (0 0 1) facets in promoting the activity of PCO of NH_3.

4. Conclusions

Fluorinated TiO_2 nanosheets (F–TiO_2), defluorinated catalyst (D-TiO_2) and pure TiO_2 nanoparticles were prepared by using a hydrothermal method and were evaluated for the PCO of gaseous NH_3. The F–TiO_2 catalyst showed the best activity among the series of catalysts. It is shown that both the exposure of a high percentage of (0 0 1) facets and the presence of surface ≡Ti–F groups contributed to the excellent activity of F–TiO_2, but the surface fluorination played a dominant role compared to that of the active(0 0 1) facets in enhancing the activity of the PCO of NH_3.

Acknowledgments

This work was financially supported by the Program of the Ministry of Science and Technology of China (2010AA064905), the Strategic Priority Research Program of the Chinese Academy of Sciences (No. XDB05050600) and the National Natural Science Foundation of China (21077117).

References

[1] A. Jones, Atmos. Environ. 33 (1999) 4535–4564.
[2] Z.Y. Meng, W.L. Lin, X.M. Jiang, P. Yan, Y. Wang, Y.M. Zhang, X.F. Jia, X.L. Yu, Atmos. Chem. Phys. 11 (2011) 6139–6151.
[3] Z. Bai, Y. Dong, Z. Wang, T. Zhu, Environ. Int. 32 (2006) 303–311.
[4] K. Kim, C. Shin, Carbon Sci. 2 (2001) 109–112.
[5] A. Akah, C. Cundy, A. Garforth, Appl. Catal., B 59 (2005) 221–226.
[6] X.Z. Cui, J. Zhou, Z.Q. Ye, H.R. Chen, L. Li, M.L. Ruan, J.L. Shi, J. Catal. 270 (2010) 310–317.
[7] L. Zhang, H. He, J. Catal. 268 (2009) 18–25.
[8] F.N. Chen, X.D. Yang, Q. Wu, Environ. Sci. Technol. 43 (2009) 4606–4611.
[9] J. Mo, Y. Zhang, Q. Xu, J.J. Lamson, R. Zhao, Atmos. Environ. 43 (2009) 2229–2246.
[10] T. Guo, Z. Bai, C. Wu, T. Zhu, Appl. Catal., B 79 (2008) 171–178.
[11] C. Chen, W. Ma, J. Zhao, Chem. Soc. Rev. 39 (2010) 4206–4219.
[12] H. Hou, H. Miyafuji, H. Kawamoto, S. Saka, J. Wood Sci. 52 (2006) 533–538.
[13] M. Nazir, J. Takasaki, H. Kumazawa, Chem. Eng. Commun. 190 (2003) 322–333.
[14] Y.C. Dong, Z.P. Bai, R.H. Liu, T. Zhu, Atmos. Environ. 41 (2007) 3182–3192.
[15] Y.C. Dong, Z.P. Bai, R.H. Liu, T. Zhu, Catal. Today 126 (2007) 320–327.
[16] Q.J. Geng, Q.J. Guo, C.Q. Cao, Y.C. Zhang, L.T. Wang, Ind. Eng. Chem. Res. 47 (2008) 4363–4368.
[17] Q.J. Geng, X.K. Wang, S.F. Tang, Biomed. Environ. Sci. 21 (2008) 118–123.
[18] P.A. Kolinko, D.V. Kozlov, Appl. Catal., B 90 (2009) 126–131.
[19] S. Yamazoe, T. Okumura, Y. Hitomi, T. Shishido, T. Tanaka, J. Phys. Chem. C 111 (2007) 11077–11085.
[20] S. Yamazoe, T. Okumura, T. Tanaka, Catal. Today 120 (2007) 220–225.
[21] H.G. Yang, C.H. Sun, S.Z. Qiao, J. Zou, G. Liu, S.C. Smith, H.M. Cheng, G.Q. Lu, Nature 453 (2008) 638–641.
[22] X.Q. Gong, A. Selloni, J. Phys. Chem. B 109 (2005) 19560–19562.
[23] Q. Xiang, K. Lv, J. Yu, Appl. Catal., B 96 (2010) 557–564.
[24] H.G. Yang, G. Liu, S.Z. Qiao, C.H. Sun, Y.G. Jin, S.C. Smith, J. Zou, H.M. Cheng, G.Q. Lu, J. Am. Chem. Soc. 131 (2009) 4078–4083.
[25] D.Q. Zhang, G.S. Li, X.F. Yang, J.C. Yu, Chem. Commun. (2009) 4381–4383.
[26] J. Zhang, J. Wang, Z. Zhao, T. Yu, J. Feng, Y. Yuan, Z. Tang, Y. Liu, Z. Li, Z. Zou, Phys. Chem. Chem. Phys. 14 (2012) 4763–4769.
[27] Y. Zhao, Q. Zhao, X. Li, Y. Hou, X. Zou, J. Wang, T. Jiang, T. Xie, Mater. Lett. 66 (2012) 308–310.
[28] Y. Zheng, K. Lv, Z. Wang, K. Deng, M. Li, J. Mol. Catal. A: Chem. 356 (2012) 137–143.
[29] Z. Zheng, B. Huang, X. Qin, X. Zhang, Y. Dai, M. Jiang, P. Wang, M.H. Whangbo, Chem. Eur. J. 15 (2009) 12576–12579.
[30] S. Liu, J. Yu, M. Jaroniec, Chem. Mater. 23 (2011) 4085–4093.
[31] M. Lazzeri, A. Vittadini, A. Selloni, Phys. Rev. B: Condens. Matter 63 (2001) 155409.
[32] K. Lv, B. Cheng, J. Yu, G. Liu, Phys. Chem. Chem. Phys. 14 (2012) 5349–5362.
[33] K. Lv, Q. Xiang, J. Yu, Appl. Catal., B 104 (2011) 275–281.
[34] X.G. Han, Q. Kuang, M.S. Jin, Z.X. Xie, L.S. Zheng, J. Am. Chem. Soc. 131 (2009) 3152–3153.
[35] F. Tian, Y. Zhang, J. Zhang, C. Pan, J. Phys. Chem. C 116 (2012) 7515–7519.
[36] J. Pan, G. Liu, G.M. Lu, H.M. Cheng, Angew. Chem. Int. Ed. 50 (2011) 2133–2137.
[37] T.R. Gordon, M. Cargnello, T. Paik, F. Mangolini, R.T. Weber, P. Fornasiero, C.B. Murray, J. Am. Chem. Soc. 134 (2012) 6751–6761.
[38] J. Yu, S. Liu, H. Yu, J. Catal. 249 (2007) 59–66.
[39] J. Yu, W. Wang, B. Cheng, B.-L. Su, J. Phys. Chem. C 113 (2009) 6743–6750.
[40] H. Park, W. Choi, J. Phys. Chem. B 108 (2004) 4086–4093.
[41] M. Herrmann, U. Kaluza, H. Boehm, Z. Anorg. Allg. Chem. 372 (1970) 308–313.
[42] M.S. Vohra, S. Kim, W. Choi, J. Photochem. Photobiol., A 160 (2003) 55–60.
[43] C. Minero, G. Mariella, V. Maurino, E. Pelizzetti, Langmuir 16 (2000) 2632–2641.
[44] C. Minero, G. Mariella, V. Maurino, D. Vione, E. Pelizzetti, Langmuir 16 (2000) 8964–8972.
[45] J.C. Yu, J. Yu, W. Ho, Z. Jiang, L. Zhang, Chem. Mater. 14 (2002) 3808–3816.
[46] Q. Wang, C. Chen, D. Zhao, W. Ma, J. Zhao, Langmuir 24 (2008) 7338–7345.
[47] J. Shi, J. Chen, Z. Feng, T. Chen, Y. Lian, X. Wang, C. Li, J. Phys. Chem. C 111 (2007) 693–699.
[48] X.F. Chen, X.C. Wang, Y.D. Hou, J.H. Huang, L. Wu, X.Z. Fu, J. Catal. 255 (2008) 59–67.
[49] Z.L. He, Z.F. Zhu, J.Q. Li, J.Q. Zhou, N. Wei, J. Hazard. Mater. 190 (2011) 133–139.
[50] J.G. Yu, T.T. Ma, S.W. Liu, Phys. Chem. Chem. Phys. 13 (2011) 3491–3501.
[51] A. Selloni, Nat. Mater. 7 (2008) 613–615.